Uncertainty of droplet evaporation measurements and its effect on model validation

D. Csemány[*] and V. Józsa

Department of Energy Engineering, Faculty of Mechanical Engineering, Budapest University of Technology and Economics, H-1111 Budapest, Műegyetem rkp. 3.

Abstract

Measurement of droplet evaporation is challenging since the average practical droplet size is too small, thus single droplets with a larger diameter are usually investigated. However, measurement data often bears notable uncertainty or bias, encumbering model validation. Therefore, typical conditions of evaporation measurements are evaluated by numerical modeling, and the results are compared to experimental data of n-heptane droplets. Vaporization rate of millimeter-scale droplets is considerably enhanced at high temperature due to thermal radiation. Heat balance of droplet is dominated by convective heat transfer at the early, and heat conduction through the suspension fiber in the late vaporization period. However, fiber conduction has no significant impact on vaporization below a certain fiber-to-droplet initial diameter ratio.

Introduction

The energy and transportation sector of the world is highly dependent on combustion systems, and the demand is still increasing. Therefore, efficient combustion of liquid fuels is crucial in order to meet the latest pollutant emission standards and provide efficient operation. In addition, several alternative liquid fuels came up in the past decades which should be utilized locally to have a positive energy balance [1,2]. The droplets generated via atomization need to be evaporated and mixed with combustion air before reaching the flame front. To optimize combustion chamber design, the evaporation process is analyzed by computational methods [3–5]. The applied models are developed based on extensive experimental data. However, the measurement of droplet spray evaporation is difficult due to a large number of tiny droplets which need to be tracked. Hence, the measurement of a single droplet with a larger diameter is usually performed as the fundamental physical phenomena are identical. Nomura et al. [6] and Chauveau et al. [7] analyzed the evaporation characteristics in microgravity. Verwey [8] evaluated the effect of natural convection on the vaporization of small droplets, while Nguyen et al. [9] investigated binary mixture droplets in gas flow. The effects of swelling and puffing during the evaporation of droplets were investigated by several authors. Wang et al. [10] carried out measurements of jatropha oil droplets, while Yang et al. [11] and Kim et al. [12] investigated high-viscosity gel and emulsion fuel droplets. These measurement methods can be divided into two main groups, depending on the motion of the droplet: suspended droplet and drop-tower methods [13,14].

Suspended droplet method is generally used due to its practical advantages. The droplet is stagnant, thus the effect of forced convection on vaporization is eliminated. A fixed high-speed camera can easily detect the temporal variation of droplet diameter. The suspension of the droplet can be either a silica fiber or a thermocouple. However, larger, typically millimeter-scale droplets are more sensitive to thermal radiation from the high-temperature environment, i.e., surfaces and the surrounding gas. Therefore, thermal shielding is commonly applied [15]. Another biasing factor is the heat conduction through the suspension system, since the thermal conductivity of suspension fibers is usually larger by few magnitudes than the thermal conductivity of vapor-air mixture around the droplet surface, resulting in additional heat transfer from the environment to the inspected droplet [16].

Correction methods considering fiber thermal conduction towards the droplet can be divided into two groups. The first method introduces a correction factor for the steady-state evaporation rate [16,17] that characterizes the steepness of the temporal variation of squared diameter of the droplet which is the D^2-law [4]. Hence, the theoretical value of steady-state evaporation rate constant, which can be calculated from the gas phase models, is corrected by an empirical term that depends on the temperature, fiber diameter, and material properties of the droplet and fiber. This way, all the effects that disturb the temporal variation of droplet diameter can be eliminated for the actual measurement setup. The second method for correction is considering the fiber thermal conduction as a source term in the heat balance of the droplet, assuming that heat transferred by conduction towards the droplet is homogeneously distributed in the droplet volume [18,19].

Tracking the temporal variation of droplet diameter in drop-tower experiments is more challenging and demands novel experimental apparatus, however, this method bears several advantages. As the droplet is moving, there is no need for a suspension system; thus fiber conduction does not affect vaporization. The effect of forced convection is minimized by adjusting the ambient gas velocity resulting in low Reynolds numbers [14]. The droplet size is usually smaller than that of suspended droplets, however, thermal radiation may still influence vaporization.

In the present work, both thermal radiation and fiber conduction are considered as source terms in the heat balance of droplet. With this correction method, the

---

[*] Corresponding author: csemany@energia.bme.hu

conclusions derived later are more general. A classical layout of suspended single droplet measurement is considered as a horizontal fiber with the droplet on its tip, shown in **Fig. 1**. The evaporation model is detailed in the upcoming section.

Evaporation model

The fundamental equations of the present droplet vaporization model are widely used in commercial numerical codes [20]. Hence, only the key details and modifications are described below.

Figure 2 shows the numerical algorithm of the evaporation model. Firstly, the boundary and initial conditions such as ambient gas pressure and temperature, initial droplet diameter and temperature and material constants such as parameters of Lennard-Jones potential for binary diffusion coefficient are specified. Then the model parameters, e.g., time step are defined. The relevant pressure and temperature-dependent thermophysical properties of n-heptane and ambient gas are downloaded from the NIST database [21].
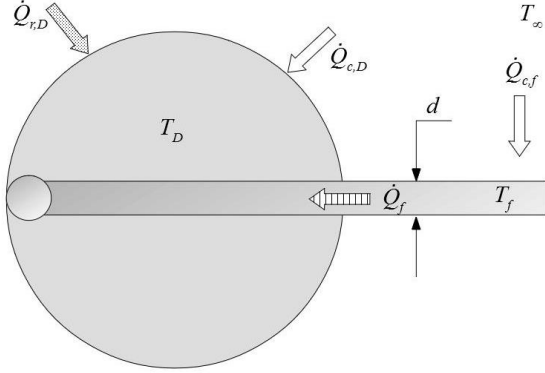

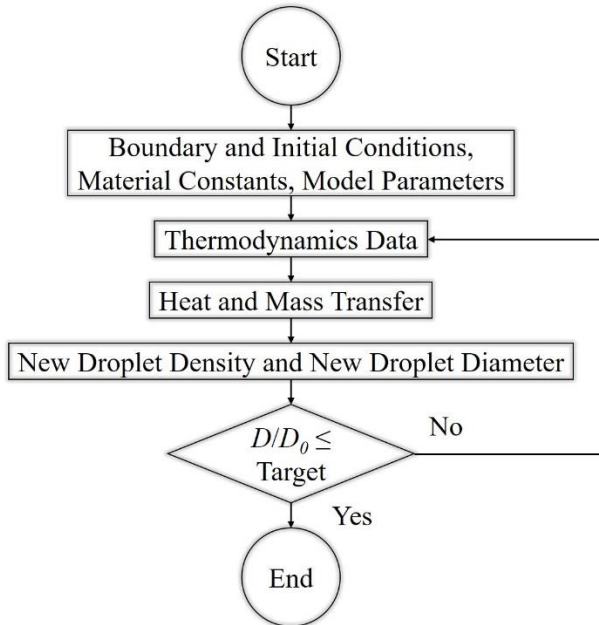**Fig. 1.** Geometric model of a suspended single droplet.

Fig. 2. The numerical algorithm of the used evaporation model.

The calculation of Spalding mass transfer and heat transfer numbers are defined by Eqs. (1) and (2):

$$B_M = \frac{Y_{vs} - Y_{v\infty}}{1 - Y_{vs}}, \tag{1}$$

$$B_T = (1 + B_M)^{\frac{c_{pv}}{c_{pg}} \frac{1}{Le}} - 1, \tag{2}$$

where Y_{vs}, $Y_{v\infty}$, c_{pv}, and c_{pg} are the mass fraction of vapor at the droplet surface and in the ambient gas and specific heat capacity of vapor and vapor-ambient gas mixture, respectively. Le is the Lewis number. The mass flow rate of evaporation considering the effect of Stefan flow is:

$$\dot{m}_D = 2\pi D D_v \rho_g \ln(1 + B_M), \tag{3}$$

where D, D_v, and ρ_g are the droplet diameter, binary diffusion coefficient and density of the vapor-ambient gas mixture, respectively. The Nusselt number of the droplet is:

$$Nu = \frac{\ln(1 + B_T)}{B_T} Nu_0, \tag{4}$$

where Nu_0 is the Nusselt number for a non-evaporating sphere. Nu_0 is calculated by Eq. (5) for stagnant droplet (natural convection) and by Eq. (6) for moving droplet (forced convection) [22]:

$$Nu_0 = 2 + 0.56 \left(\frac{Pr Ra_D}{0.846 + Pr}\right)^{0.25}, \tag{5}$$

$$Nu_0 = 2 + 0.6 Re_D^{1/2} Pr^{1/3}, \tag{6}$$

where Pr is the Prandtl number, Ra_D and Re_D are the droplet Rayleigh and Reynolds numbers, respectively. The temperature of the droplet and the temperature of the fiber at the end of the time step are calculated by Eqs. (7) and (8):

$$m_D c_{pl} \frac{dT_D}{dt} = \dot{Q}_{c,D} - \dot{m}_D L + \dot{Q}_{r,D} + \dot{Q}_f, \tag{7}$$

$$m_f c_f \frac{dT_f}{dt} = \dot{Q}_{c,f} - \dot{Q}_f, \tag{8}$$

where c_{pl} and c_f are the specific heat capacity of droplet and fiber respectively, m, is the mass, and T is the temperature. Subscripts D and f refer to droplet and fiber. L is the latent heat of vaporization. The further source terms of Eqs. (7) and (8) are defined by Eqs. (9)–(12). The rate of convective heat flow to the droplet:

$$\dot{Q}_{c,D} = -h_D D^2 \pi (T_D - T_\infty), \tag{9}$$

where h_D is the droplet heat transfer coefficient, and T_∞ is the ambient gas temperature. The rate of radiative heat flow to the droplet:

$$\dot{Q}_{r,D} = D^2 \pi \varepsilon \varphi \sigma_0 (\theta_r^4 - T_D^4), \tag{10}$$

where ε is the mutual absorption coefficient, φ is the view factor, Θ_r is the radiation temperature respectively, and σ_0 is the Stefan-Boltzmann constant. In the case of optically thick gases, radiation temperature is considered equal to the ambient gas temperature [3,23]. Assuming one-dimensional heat conduction in the fiber, the rate of heat flow by conduction through the fiber according to Fourier's law:

$$\dot{Q}_f = -k_f \frac{d^2\pi}{4}\frac{(T_D - T_f)}{D/2}, \qquad (11)$$

where k_f and d are the thermal conductivity and the diameter of the fiber, respectively. The total rate of heat flow towards the droplet is the sum of Eqs. (9)–(11). The rate of convective heat flow to the fiber from the environment:

$$\dot{Q}_{c,f} = -h_f d\pi \left(H + \frac{D_0}{2} - \frac{D}{2}\right)\left(T_f - T_\infty\right), \qquad (12)$$

where h_f and H are the heat transfer coefficient and length of the fiber, respectively.

A droplet expands as its temperature increases during the heat-up period as an effect of the decrease in liquid density. Therefore, the liquid density needs to be updated at the end of each time step with the new droplet temperature. Then the new droplet diameter is calculated with the integral mean value of droplet density in order to model the swelling effect. If the ratio of D/D_0 has reached a predetermined value, where D_0 is the initial droplet diameter, calculation stops.

Results and discussion

Figures 3 and **4** show the comparison of the discussed evaporation model and the experimental data of Nomura et al. [13] and Ghassemi et al. [15] for 10 bar ambient pressure and several ambient temperatures for stagnant, suspended droplets. The effect of thermal radiation was investigated by a parameter analysis. Dashed lines indicate $\varepsilon \cdot \varphi = 0$ which mean no radiation, while solid lines indicate $\varepsilon \cdot \varphi = 1$, meaning that all the radiated heat from the surrounding gas reaches the droplet. Identifying the value of $\varepsilon \cdot \varphi$ for a given measurement setup is often a difficult task since ε is a function of the temperature [24], and φ is rarely published for all parts of the test equipment. Therefore, determining the limits of radiative heat transfer is reasonable for evaluating its effect on droplet evaporation. As the effect of thermal radiation is influenced by the size of the droplet and the ambient temperature as well, either the droplet diameter or the ambient temperature is increased, the sensitivity range widens; thus the measurement is increasingly biased, shown in **Figs. 3** and **4**. If the 669 K $\leq T_\infty \leq$ 773 K data sets are compared in **Figs. 3** and **4**, the only notable difference which affects thermal radiation is the initial droplet diameter, as ambient temperatures are practically identical for the 2-2 cases with similar temperatures. Thermal radiation affects more the evaporation of the larger droplet than that of the smaller droplet.
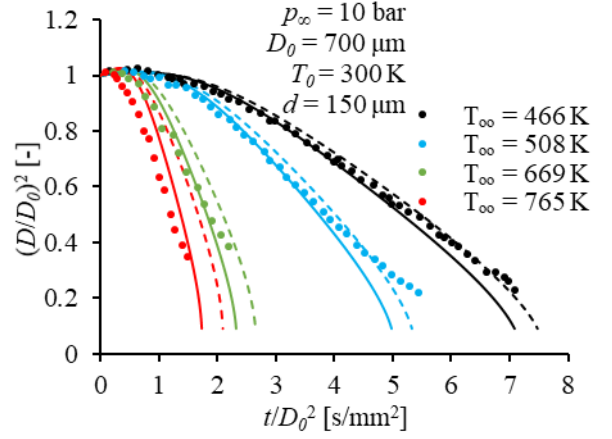

Fig. 3. Comparison of the evaporation model and the experimental data of Nomura et al. [13]. Dashed lines indicate $\varepsilon \cdot \varphi = 0$, solid lines indicate $\varepsilon \cdot \varphi = 1$.
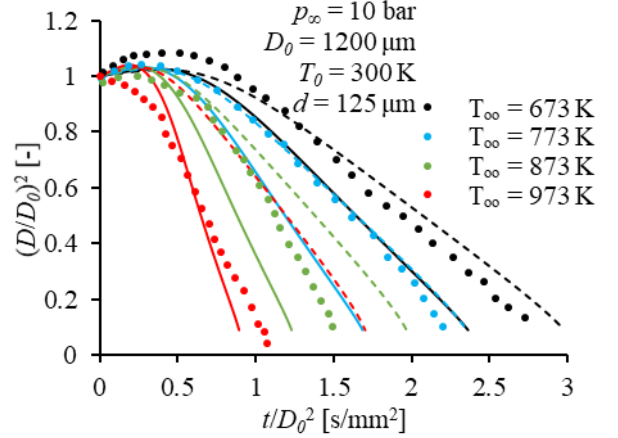

Fig. 4. Comparison of the evaporation model and the experimental data of Ghassemi et al. [15]. Dashed lines indicate $\varepsilon \cdot \varphi = 0$, solid lines indicate $\varepsilon \cdot \varphi = 1$.

Figure 5 compares two extreme cases considering the typical limiting conditions of droplet evaporation measurement. A small diameter droplet evaporates in a low ambient temperature environment while the other case considers a larger droplet in a high-temperature environment. Calculations performed until the droplet diameter decreased to 30 % of the initial value. This limit is frequently used in measurement of single droplet evaporation due to the finite size of the tip. The corresponding evaporation time is noted as $t_{D70\%}$ which is used for the non-dimensional time coordinate, $t/t_{D70\%}$. Presently, the effect of conduction of fiber is neglected. The low-temperature case shows low sensitivity to radiation in **Fig. 5**, even for $\varepsilon \cdot \varphi = 1$, the share of thermal radiation in the total heat flow rate is below 10%. However, in the second case, depending on the value of $\varepsilon \cdot \varphi$, the share of thermal radiation in the total heat flow rate can reach up to 90%. Hence, thermal radiation may considerably influence the measurements in the case of millimeter-scale droplets, and high temperature may seriously enhance its impact.
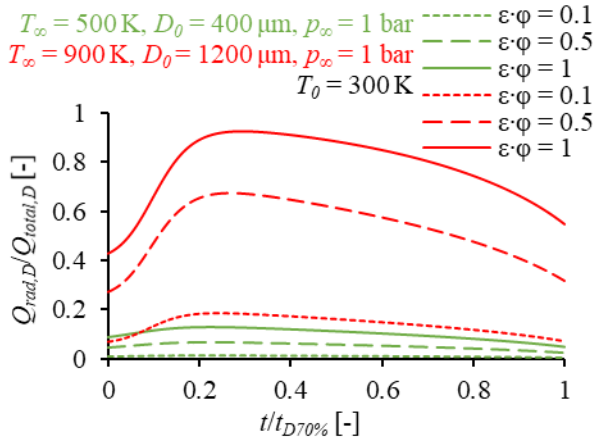
Fig. 5. Share of thermal radiation in total heat transfer during droplet vaporization for two initial conditions. The effect of the fiber is omitted.

Figure 6 shows the comparison of the evaporation model and the experimental data of Chung [14] for moving droplets. As notable uncertainty biased the initial temperature of the droplets, T_0, only the steady-state evaporation period was evaluated from a thermal radiation point of view. The impact of thermal radiation on droplet vaporization is present; however, it is less significant despite the high, combustion chamber-like far-field temperature due to the considerably smaller droplet size than those discussed above. Therefore, in real fuel sprays, where droplet size is usually below 50 μm, thermal radiation may be omitted even in a high-temperature environment.
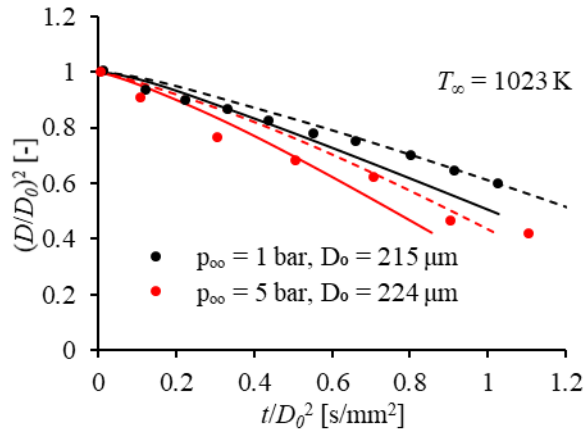

Fig. 6. Comparison of the evaporation model and the experimental data of Chung [14]. Dashed lines indicate $\varepsilon \cdot \varphi = 0$, solid lines indicate $\varepsilon \cdot \varphi = 1$.

In order to evaluate the share of different sources of heat transfer in total heat transfer, an experimental setup identical for Ghassemi et al. [15] was chosen with $\varepsilon \cdot \varphi = 0.5$. **Figure 7** shows the convective heat transfer dominates the early vaporization period while thermal radiation has a moderate impact. The effect of fiber conduction is small because the difference in droplet and fiber temperature is low. However, as the wet-bulb temperature is approached, the share of convective heat

transfer decreases since both droplet size and difference in the droplet and ambient temperature decreases. Moreover, as temperature increases, B_T increases as well. Therefore, the Nusselt number and hence the heat transfer coefficient decrease. The decrease in droplet size also impacts thermal radiation. After reaching a maximum, its share in total heat transfer starts to decrease. In this intermediate period, the role of convective heat transfer decreases while thermal radiation may increase if the droplet is large. The effect of fiber conduction becomes increasingly important since the diameter of the fiber to the diameter of the droplet is continuously increasing. Moreover, the temperature of the fiber increases and reaches a steady-state value, very close to the far field temperature. At the end of the evaporation process, when the droplet diameter is about 30 % of the initial value, fiber conduction dominates and may boil the droplet. In addition, the sphericity is also violated, and the discussed model is no longer applicable.
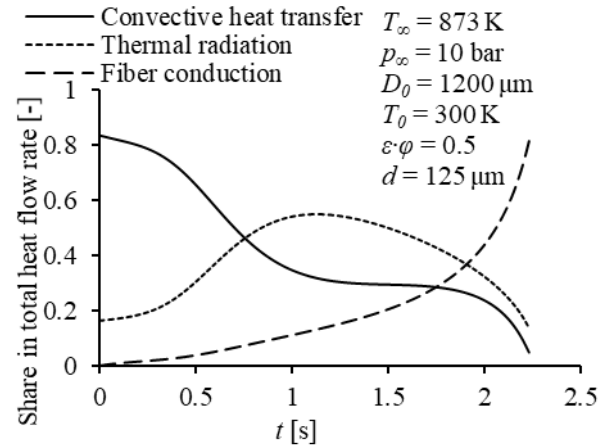

Fig. 7. The share of different sources of heat transfer in total heat flow rate during droplet vaporization.

Besides the thermal conductivity of the fiber, the other notable parameter which determines the effect of droplet suspension on the measurement is the d/D_0 ratio. **Figure 8** shows the deviation of D^2 profiles from D^2-law while **Fig. 9** shows the share of fiber conduction in the total heat transfer. The effect of thermal radiation is omitted here. Increasing the diameter ratio above 0.05 leads to a significant nonlinear behavior of the D^2 profiles since fiber conduction starts to dominate the heat balance at the end of the droplet lifetime. However, below 0.05, the effect of fiber conduction is practically negligible as the share of fiber conduction in total heat transfer is below 10% except for the very end of the droplet lifetime. Therefore, in the case of droplets with millimeter-scale initial diameter, fiber with 10-50 μm diameter has little effect on vaporization. Increasing ambient pressure decreases the temperature difference between the fiber and droplet as pressure increase has no impact on fiber temperature, thus the effect of fiber conduction is slightly decreased. Increasing ambient temperature increases the temperature difference between the fiber and droplet as fiber temperature increases, but this effect is not considerable either.
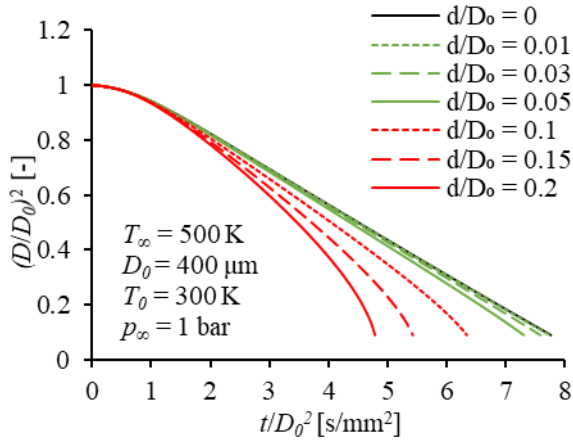
4

Fig. 8. Deviation from D^2-law for different d/D_0 ratios. The effect of thermal radiation is omitted.
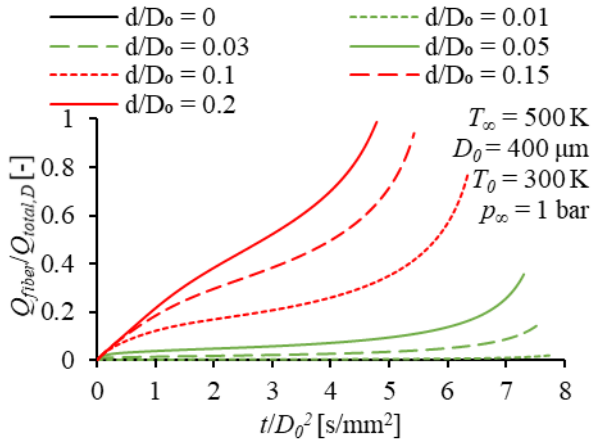

Fig. 9. Effect of d/D_0 ratio on fiber conduction.

Conclusions

Typical setups for evaporation measurement of single droplets including suspended droplet and drop-tower method were investigated from thermal point of view by numerical modeling. Heat balance of the droplet considered thermal conduction of the suspension fiber and thermal radiation. The modified numerical model was compared to available experimental data for n-heptane in the literature. The following conclusions were derived:

1. As thermal radiation is highly dependent on droplet size and ambient temperature, typical suspended single droplet evaporation measurement setups, where generally millimeter-scale droplets are investigated, may be considerably influenced by radiative heat transfer. This is enhanced in high-temperature environment, resulting in a higher vaporization rate. Hence, the importance of determining the value of $\varepsilon \cdot \varphi$ may be crucial in order to validate the results of numerical models. Drop–tower measurements are less influenced by thermal radiation, due to the typically smaller droplet sizes.

2. The early vaporization period is dominated by convective heat transfer, and, depending on the measurement setup, thermal radiation may be significant as well. However, fiber conduction is practically negligible. As vaporization progresses, the share of convection in total heat transfer decreases as droplet diameter, Nusselt number, heat transfer coefficient, and the difference in the droplet and ambient temperature decrease. Reduction in droplet size reduce the share of thermal radiation as well after reaching a maximum. At the end of the evaporation process, when the fiber diameter is comparable to the droplet diameter, fiber conduction dominates. In addition, the sphericity might require adaptive modeling approaches for the possibly distorting liquid shape.

3. Above $d/D_0 = 0.05$, a significant nonlinear behavior can be observed in the D^2 profiles due to the dominance of fiber conduction in the heat balance of the droplet close to the end of the vaporization process. However, below $d/D_0 = 0.05$, fiber conduction has no significant impact on evaporation as its share in the total heat flow rate is below 10% except for the late vaporization period.

References

[1] O'Connell A, Kousoulidou M, Lonza L, Weindorf W. Considerations on GHG emissions and energy balances of promising aviation biofuel pathways. Renew Sustain Energy Rev 2019;101:504–15. doi:https://doi.org/10.1016/j.rser.2018.11.033.

[2] Correa DF, Beyer HL, Fargione JE, Hill JD, Possingham HP, Thomas-Hall SR, et al. Towards the implementation of sustainable biofuel production systems. Renew Sustain Energy Rev 2019;107:250–63. doi:https://doi.org/10.1016/j.rser.2019.03.005.

[3] Sazhin S. Droplets and Sprays. 2014. doi:10.1007/978-1-4471-6386-2.

[4] Lefebvre AH, McDonell VG. Atomization and Sprays. Second Edi. Boca Raton: CRC Press, Taylor & Francis Group; 2017.

[5] Sirignano WA. Fluid Dynamics and Transport of Droplets and Sprays. Second. New York: Cambridge University Press; 2010.

[6] Nomura H, Murakoshi T, Suganuma Y, Ujiie Y, Hashimoto N, Nishida H. Microgravity experiments of fuel droplet evaporation in sub- and supercritical environments. Proc Combust Inst 2017;36:2425–32. doi:https://doi.org/10.1016/j.proci.2016.08.046.

[7] Chauveau C, Birouk M, Gökalp I. An analysis of the d2-law departure during droplet evaporation in microgravity. Int J Multiph Flow 2011;37:252–9. doi:https://doi.org/10.1016/j.ijmultiphaseflow.2010.10.009.

[8] Verwey C, Birouk M. Experimental investigation of the effect of natural convection on the evaporation characteristics of small fuel droplets at moderately elevated temperature and pressure. Int J Heat Mass Transf 2018;118:1046–55. doi:https://doi.org/10.1016/j.ijheatmasstransfer.2017.11.038.

[9] Nguyen TTB, Mitra S, Sathe MJ, Pareek V, Joshi JB, Evans GM. Evaporation of a suspended binary mixture droplet in a heated flowing gas stream. Exp Therm Fluid Sci 2018;91:329–44. doi:https://doi.org/10.1016/j.expthermflusci.2017.10.025.

[10] Wang J, Wang X, Chen H, Jin Z, Xiang K. Experimental study on puffing and evaporation characteristics of jatropha straight vegetable oil (SVO) droplets. Int J Heat Mass Transf 2018;119:392–9. doi:https://doi.org/10.1016/j.ijheatmasstransfer.2017.11.130.

[11] Yang D, Xia Z, Huang L, Ma L, Feng Y, Xiao Y. Exprimental study on the evaporation characteristics of the kerosene gel droplet. Exp Therm Fluid Sci 2018;93:171–7. doi:https://doi.org/10.1016/j.expthermflusci.2017.12.031.

[12] Kim H, Won J, Baek SW. Evaporation of a single emulsion fuel droplet in elevated temperature and pressure conditions. Fuel 2018;226:172–80. doi:https://doi.org/10.1016/j.fuel.2018.04.010.

[13] Nomura H, Ujiie Y, Rath HJ, Sato J, Kono M. Experimental study on high-pressure droplet evaporation using microgravity conditions. Symp Combust 1996;26:1267–73. doi:https://doi.org/10.1016/S0082-0784(96)80344-4.

[14] Chung SS, Kawaguchi O. Evaporation Rate of Free Paraffin Hydrocarbon Droplets in a High-Temperature and High-Pressure Gas Stream. JSME Int J Ser B 1995;38:121–8. doi:10.1299/jsmeb.38.121.

[15] Ghassemi H, Baek S, Sarwar Khan Q. Experimental study on binary droplet evaporation at elevated pressures and temperatures. vol. 178. 2006. doi:10.1080/00102200500296697.

[16] Chauveau C, Birouk M, Halter F, Gökalp I. An analysis of the droplet support fiber effect on the evaporation process. Int J Heat Mass Transf 2019;128:885–91. doi:https://doi.org/10.1016/j.ijheatmasstransfer.2018.09.029.

[17] Chauveau C, Halter F, Lalonde A, Gökalp I. An experimental study on the droplet vaporization: effects of heat conduction through the support fiber. IT 2008. 2008.

[18] Strizhak PA, Volkov RS, Castanet G, Lemoine F, Rybdylova O, Sazhin SS. Heating and evaporation of suspended water droplets: Experimental studies and modelling. Int J Heat Mass Transf 2018;127:92–106. doi:https://doi.org/10.1016/j.ijheatmasstransfer.2018.06.103.

[19] Han K, Song G, Ma X, Yang B. An experimental and theoretical study of the effect of suspended thermocouple on the single droplet evaporation. Appl Therm Eng 2016;101:568–75. doi:https://doi.org/10.1016/j.applthermaleng.2015.12.022.

[20] Ansys Fluent Theory Guide 2019 R1.

[21] Lemmon EW, McLinden MO, Friend DG. Thermophysical Properties of Fluid Systems, NIST Chemistry WebBook, NIST Standard Reference Database Number 69 n.d. doi:doi:10.18434/T4D303.

[22] VDI Heat Atlas. Second. 2010. doi:10.1007/978-3-540-77877-6.

[23] Szőke A, Brooks III ED. The transport equation in optically thick media. J Quant Spectrosc Radiat Transf 2005;91:95–110. doi:https://doi.org/10.1016/j.jqsrt.2004.06.001.

[24] Dombrovsky LA, Sazhin SS, Sazhina EM, Feng G, Heikal MR, Bardsley MEA, et al. Heating and evaporation of semi-transparent diesel fuel droplets in the presence of thermal radiation. Fuel 2001;80:1535–44. doi:https://doi.org/10.1016/S0016-2361(01)00025-4.